



## NRC Publications Archive Archives des publications du CNRC

### **Cold spray deposition of Ni and WC-reinforced Ni matrix composite coatings**

Alidokht, S. A.; Vo, P.; Yue, S.; Chromik, R. R.

This publication could be one of several versions: author's original, accepted manuscript or the publisher's version. / La version de cette publication peut être l'une des suivantes : la version prépublication de l'auteur, la version acceptée du manuscrit ou la version de l'éditeur.

For the publisher's version, please access the DOI link below. / Pour consulter la version de l'éditeur, utilisez le lien DOI ci-dessous.

#### **Publisher's version / Version de l'éditeur:**

<https://doi.org/10.1007/s11666-017-0636-4>

*Journal of Thermal Spray Technology*, 26, 8, pp. 1908-1921, 2017-09-07

#### **NRC Publications Record / Notice d'Archives des publications de CNRC:**

<https://nrc-publications.canada.ca/eng/view/object/?id=588aec92-33c6-4e7e-989e-635763c6669a>

<https://publications-cnrc.canada.ca/fra/voir/objet/?id=588aec92-33c6-4e7e-989e-635763c6669a>

Access and use of this website and the material on it are subject to the Terms and Conditions set forth at

<https://nrc-publications.canada.ca/eng/copyright>

READ THESE TERMS AND CONDITIONS CAREFULLY BEFORE USING THIS WEBSITE.

L'accès à ce site Web et l'utilisation de son contenu sont assujettis aux conditions présentées dans le site

<https://publications-cnrc.canada.ca/fra/droits>

LISEZ CES CONDITIONS ATTENTIVEMENT AVANT D'UTILISER CE SITE WEB.

**Questions?** Contact the NRC Publications Archive team at

PublicationsArchive-ArchivesPublications@nrc-cnrc.gc.ca. If you wish to email the authors directly, please see the first page of the publication for their contact information.

**Vous avez des questions?** Nous pouvons vous aider. Pour communiquer directement avec un auteur, consultez la première page de la revue dans laquelle son article a été publié afin de trouver ses coordonnées. Si vous n'arrivez pas à les repérer, communiquez avec nous à PublicationsArchive-ArchivesPublications@nrc-cnrc.gc.ca.



# Cold Spray Deposition of Ni and WC-Reinforced Ni Matrix Composite Coatings

S. A. Alidokht<sup>1</sup> · P. Vo<sup>2</sup> · S. Yue<sup>1</sup> · R. R. Chromik<sup>1</sup>

Submitted: 7 March 2017 / in revised form: 24 August 2017 / Published online: 7 September 2017  
© ASM International 2017

**Abstract** Ni-WC composites are ideal protective coatings against wear and are often fabricated using laser cladding and thermal spray processes, but the high temperatures of these processes result in decarburization, which deteriorates the performance of the coating. Cold spray has the potential to deposit Ni-WC composite coatings and retain the composition of the initial WC feedstock. However, the insignificant plastic deformation of hard WC particles makes it difficult to build up a high WC content coating by cold spray. By using three different WC powder sizes, the effect of feedstock powder size on WC retention was tested. To improve WC retention, a WC/Ni composite powder in mixture with Ni was also sprayed. Microstructural characterization, including the deformed structure of Ni splats, retention, distribution, and fragmentation of WC, was performed by scanning electron microscopy. An improvement in WC retention was achieved using finer WC particles. Significant improvement in WC particles retention was achieved using WC/Ni composite powder, with the WC content in the coating being close to that of the feedstock.

**Keywords** cold spraying · hardness · metal matrix composite · WC

## Introduction

Hard composite coatings containing WC in a metal matrix are widely used due to a good combination of hardness, toughness, and improved wear resistance (Ref 1, 2). Coatings with Ni as the matrix are widely applied when wear resistance combined with oxidation or hot corrosion resistance is required (Ref 3, 4). Studies by Wang et al. (Ref 5) and Kulu and Pihl (Ref 6) showed that the wear resistance of Ni coatings can be greatly improved by the incorporation of refractory carbides, such as WC, WC-Co, TiC, and CrC. These coatings are conventionally deposited using high-temperature thermal spray and laser cladding processes. However, the high temperatures of these processes cause dissolution of carbides into the molten binder phase, thermal dissociation of WC, and loss of carbon (Ref 5-8). The result is that brittle phases such as  $W_2C$ , W and/or  $Co_6W_6C$  or  $Co_3W_3C$   $\eta$  phases are present in the coating, especially at carbide/metal interfaces. The presence of these defects has been found to increase the hardness of the coating. However, failure along the preferential crack paths provided by brittle phases intensifies material removal and decreases the wear properties of the coatings (Ref 1, 2, 8).

Cold spray is a solid-state thermal spray process where particles are accelerated through a de Laval nozzle to supersonic velocities (500-1200 m/s) in a gas stream and impact a substrate. Particles remain in solid state due to a short contact time with the gas being at a much lower temperature than the melting points of the particles. Hence, high-temperature induced decomposition of carbides and/or other phase transformations that can be avoided (Ref 9, 10). The continuous high-velocity impact of particles may produce a shot-peening or “tamping” effect, which results in densification and deposition of a coating with nearly theoretical density (Ref 11). This makes cold spray a

✉ S. A. Alidokht  
sima.ahmadalidokht@mail.mcgill.ca

<sup>1</sup> Department of Mining and Materials Engineering, McGill University, M.H. Wong Building, 3610 University Street, Montreal, QC H3A 0C5, Canada

<sup>2</sup> National Research Council Canada, 75, boul. de Mortagne, Boucherville, QC J4B 6Y4, Canada

promising replacement for traditional techniques when spraying heat-sensitive materials.

There are generally two approaches for using cold spray to fabricate metal matrix composite coatings: (a) pretreatment powder processing such as cladding (Ref 12) and sintering (Ref 13–17), and (b) spraying mechanical blends of two or more powders (Ref 18–25). For mechanically blended ceramic and metallic powders, previous researchers reported co-deposition of metallic particles with oxides and carbides. SiC or Al<sub>2</sub>O<sub>3</sub> are frequently used as reinforcement particles (Ref 18–23). Angular ceramic particles were sprayed in most of the studies (Ref 18–20), although there are also some reports available on spherical particles (Ref 24, 25). The deposition efficiency (DE) of ceramic particles in metal–ceramic mixtures strongly depends on the size and shape of ceramic particles, the hardness of the metallic particles, and the initial feedstock composition (Ref 18–25). Finer ceramic particles were more likely to embed into the substrate, which can be attributed to higher velocities attained in the gas stream (Ref 18–20). However, very small particles are difficult to deposit because of the bow shock effect at the substrate (Ref 20). Particles morphology has an effect with the retention of angular ceramic particles reported to be higher than spherical particles of the same size (Ref 25). Coatings with higher ceramic content were deposited with increasing ceramic content in the feedstock. However, above a critical content of ceramic particles, interactions between ceramic particles dominate, which results in decreased retention of ceramic particles. Previous studies demonstrated that Al matrix composites have been successfully co-deposited with SiC and Al<sub>2</sub>O<sub>3</sub> reinforcements using cold spray. It was reported that more than 70% of the initial SiC and Al<sub>2</sub>O<sub>3</sub> were retained in the coating (Ref 21–23). However, a much lower fraction of Al<sub>2</sub>O<sub>3</sub> feedstock particles of similar morphology was retained in a Ni matrix composite, with around 12–22% being reported (Ref 20), probably due to Ni being harder than Al. It is worth noting, for the studies presented above (Ref 20–23), even with optimized process parameters, the ceramic retained in the coating was less than in the feedstock.

Several researchers have deposited composite coatings containing WC by cold spray (Ref 12–17). More recently, low-pressure cold spray deposition of mechanically blended Ni–WC with angular WC was reported by Lioma et al. (Ref 26). High losses of WC particles were reported with only 11–29% of WC retained in the coatings (Ref 26). However, in most cases, pretreatment powder processing such as cladding (Ref 12) and sintering (Ref 13–17) was utilized to overcome difficulties regarding retention of hard WC particles within coatings. Most studies on WC containing cold-sprayed coatings have used a feedstock of agglomerated, sintered, and crushed WC/Co powders (Ref

13–17). WC/Co composite coatings with different ratios of carbide content and with nano- and micro-sized WC were deposited using nitrogen and helium. Several approaches were employed to overcome low DE and unsatisfactory bonding quality, which arises from limited deformability of WC/Co. These strategies include porous feedstock powder (Ref 13–15), sufficient binder/matrix content (Ref 16), and powder preheating prior to spray (Ref 17). A more recent approach was used in two studies conducted by Lioma et al. (Ref 26) and Melendez et al. (Ref 27), where WC/Co powders were sprayed with Ni additions in the initial feedstock using low-pressure cold spray. In both studies, irregularly shaped agglomerates of a fine Ni powder that was specially designed for cold spraying as well as an agglomerated and sintered WC–12 wt.% Co powder were used as feedstock. Although the low-pressure cold spray could recover 50–67% of feedstock WC in the coating, it was hypothesized that higher velocities attained by particles using high-pressure cold spray may be more effective in depositing a coating with more controlled WC content (Ref 26, 27).

In this work, using high-pressure cold spray, the effect of WC powder size and structure on cold spray behavior for Ni–WC systems is studied. Here, two types of WC-based powders, cast WC and agglomerated and sintered WC/Ni composite powders, are tested. The effect of WC powder sizes on WC DE and mechanical properties of the coatings are examined.

## Experimental

Grit-blasted mild steel plates (thickness of 3 mm) were used as substrates. In this study, four different powders were used as feedstock powders, commercially pure water atomized Ni (4SP-10, Novamet, Kentucky, USA), plasma spheroidized WC (TEKMAT<sup>TM</sup> WC-45, Tekna, Quebec, Canada), and agglomerated and sintered WC/Ni (AMPERIT<sup>®</sup> 547, H.C.Starck, Munich, Germany). Laser particle size analysis (LA-920, Horiba, Kyoto, Japan) was used to measure feedstock powder size distributions. Three different particle size distributions of WC,  $-60 + 20 \mu\text{m}$  ( $d_{50} = 40 \mu\text{m}$ ),  $-38 + 25 \mu\text{m}$  ( $d_{50} = 30 \mu\text{m}$ ), and  $-25 + 10 \mu\text{m}$  ( $d_{50} = 15 \mu\text{m}$ ), were tested. The designations of WC(40), WC(30), and WC(15) are used throughout this work. The Ni and WC/Ni powders had particle size ranges of  $-10 + 4 \mu\text{m}$  ( $d_{50} = 7 \mu\text{m}$ ) and  $-30 + 15 \mu\text{m}$  ( $d_{50} = 20 \mu\text{m}$ ), respectively. Figure 1 shows the morphology and size distribution of feedstock powders. Figure 1(e) shows the cross section of WC/Ni powder, with porosity revealed as dark regions.

A commercially available cold spray system (PCS-800, Plasma Giken, Saitama, Japan) was used to fabricate Ni

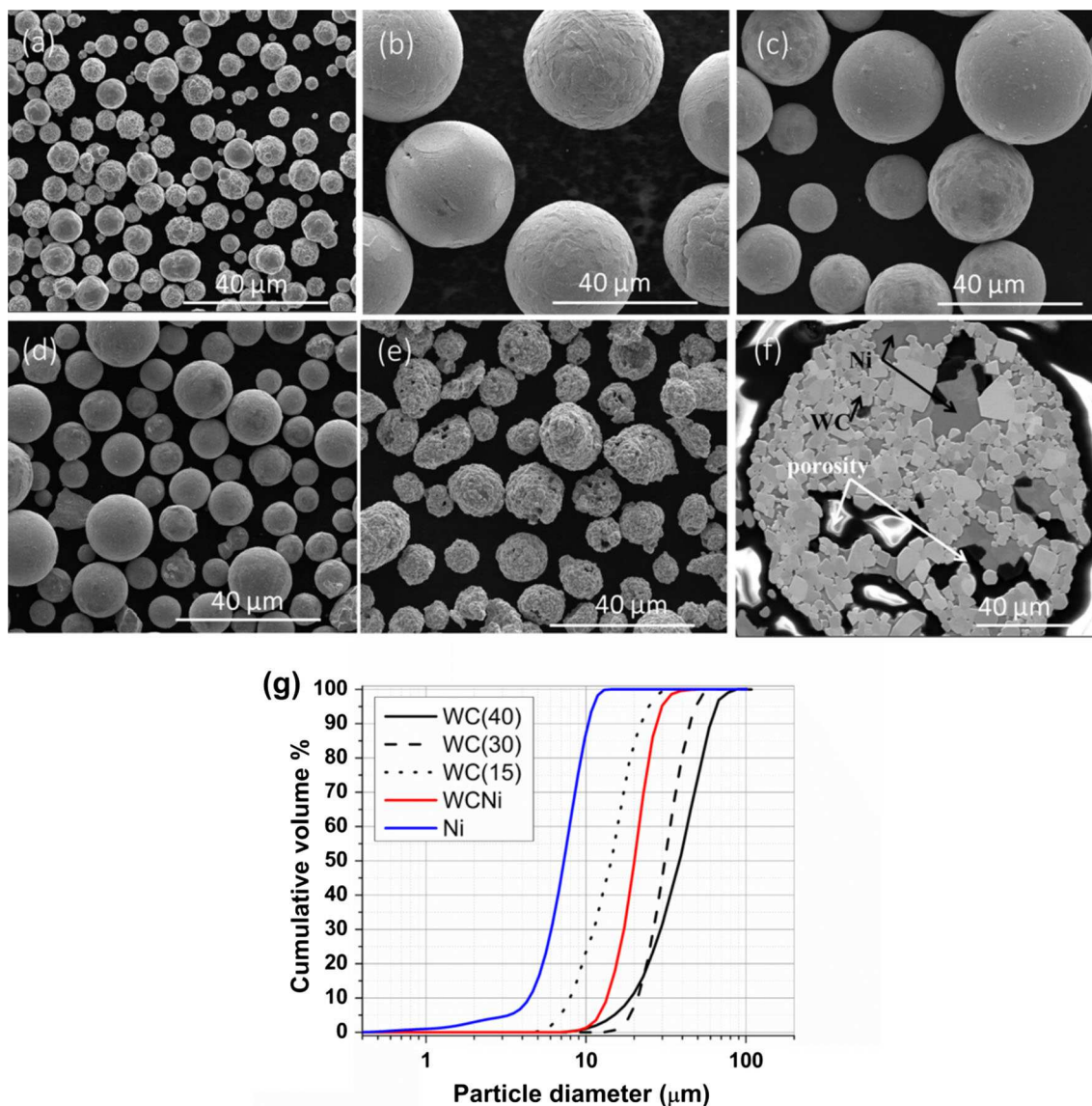


**Fig. 1** Morphology of as-received powders: (a) Ni  $-10 + 4$  ( $d_{50} = 7 \mu\text{m}$ ), (b) WC  $-45 + 15$  ( $d_{50} = 40 \mu\text{m}$ ), (c) WC  $-38 + 25$  ( $d_{50} = 30 \mu\text{m}$ ), (d) WC  $-10 + 25$  ( $d_{50} = 15 \mu\text{m}$ ),

(e) and (f) morphology and cross section of WC/Ni  $-30 + 15$  ( $d_{50} = 20 \mu\text{m}$ ), and (g) cumulative size distribution of feedstock powders

and composite coatings. The cold spray unit utilized a WC-Co, de Laval nozzle with nitrogen as the process gas. Prior to entering the nozzle, the gas pressure was 4 MPa and the gas preheat temperature was 700 °C. The standoff distance between the substrate and nozzle exit was set at 40 mm, and the gun traverse speed at 30 mm/s. The particle velocities were measured in free jet by a time-of-flight particle diagnostic system (ColdSprayMeter, Tecnar, Quebec, Canada) and are reported in Table 1. The WC and Ni powders were fed to the gun from separate hoppers. The powder feeder system was custom installed by the gun manufacturer, Plasma Giken. By setting the feed rates of powders, various mixtures of Ni-WC and WC/Ni were sprayed. The co-feeding system was used to avoid

problems arising from the difficulty in the premixing powder of differing densities and damage to powders due to mechanical mixing. Table 1 summarizes the cold spray tests parameters for each coating, feedstock powders and compositions, as well as particles velocity in the gas stream. The deposition efficiency (DE) was calculated as the weight gain divided by the mass of powder sprayed, which is a product of feed rate and spray time.

Cold-sprayed coatings were cross-sectioned perpendicular to the gun traverse direction, mechanically ground, and polished using 9, 3 and 1 μm diamond pastes followed by 0.05-μm colloidal silica. The morphology and microstructure of the initial powders and deposited coatings were observed by scanning electron microscopy (SEM) (Quanta

**Table 1** Feedstock powders and particles average velocities in the gas stream

Sample designation	Particles average velocity, m/s	Feedstock composition, vol.%
Ni	650 ± 125	100% Ni
Ni-WC ( $d_{50} = 40 \mu\text{m}$ ) —referred to as “WC(40)”	WC(40): 484 ± 78	Ni-36% WC
Ni-WC(30)	WC(30): 520 ± 73	
Ni-WC(15)	WC(15): 627 ± 135	
Ni-WC(30)	See above	Ni-36, 50, and 80% WC
Ni-WC/Ni	WC/Ni: 569 ± 108	Ni-20, 36, 50, and 76% WC

600, FEI, Oregon, USA). The WC and porosity concentrations within the coatings were measured by image analysis of pixel count using ten random SEM images of polished cross sections. Electron channeling contrast imaging (ECCI) using a cold field emission SEM (SU-8230, Hitachi, Tokyo, Japan), with a photodiode backscattered electron (BSE) detector, was performed to reveal the deformed structure of coatings.

To characterize mechanical properties of Ni powder and sprayed coatings, nano-hardness and micro-hardness testing were used. Nano-hardness testing was performed using a Berkovich diamond tip with a triboindenter system (TI 950, Hysitron, Minnesota, USA). The peak load, loading and unloading rate, and hold time at peak loads were fixed as 5 mN, 200  $\mu\text{N/s}$ , and 2 s, respectively. To calculate hardness and elastic modulus, the indentation load–displacement data during indentation were analyzed using the Oliver and Pharr method (Ref 28). Vickers micro-indentation (Clark CM-100AT, Clarke Instruments Ltd, Salisbury, UK) was performed on the top polished surfaces. To obtain an average hardness value of the composite, a large load of 1 kgf with a dwell time of 15 s on a micro-hardness tester was used. Micro-indentation was conducted on cross-sectioned WC/Ni and WC(30) powders, with a load of 25 gf and dwell time of 15 s.

## Results

### Ni Coatings

The Ni particles were accelerated to average velocities of  $650 \pm 125 \text{ m/s}$  (Table 1) and deposited onto a mild steel substrate. A Ni coating with  $1.4 \pm 0.3 \text{ mm}$  thickness, 3.8% porosity, and 55% DE was deposited by cold spray. Figure 2(a) shows the cumulative velocity distribution for Ni particles. According to the measured DE, it is possible, from this graph, to determine the critical velocity (Ref 29). The critical velocity was found to be 650–670 m/s. A high-volume fraction (50%) of particles had velocity below the critical velocity, reducing the measured DE. To obtain

higher DE, higher powder velocities are required. This can be achieved through increasing gas temperature, which not only increases particle velocity but also decreases critical velocity by improving deformability. However, high gas temperatures can cause nozzle clogging with Ni particles (Ref 20). The spray conditions in this study were selected to be the best compromise between DE and risk of nozzle clogging. Figure 2(b) and (c) shows micrographs of the cross section and the top surface of the Ni coating. Both mechanically trapped and deformed Ni particles were found in the coating (Fig. 2c), which is consistent with the range of particle velocities with respect to the critical velocity (Fig. 2a).

Figure 3(a) and (b) shows ECC images of cross-sectioned Ni powder particles and a cold-sprayed Ni coating, respectively. The grain structures of Ni powder revealed a grain size of 1–10  $\mu\text{m}$  with a mean grain size of  $4.5 \pm 0.9 \mu\text{m}$  (Fig. 3a). A non-uniform microstructure was observed for the Ni coating (Fig. 3b) with an ultra-fine microstructure near particle interfaces and a coarser structure in central regions (Fig. 3c). This is related to an inhomogeneous plastic deformation field in cold-sprayed particles, where particle/particle interfaces experience higher strains, strain rates, and adiabatic shear instabilities (Ref 30). Near the particle interfaces of the Ni coating, cell structures with a mean size of  $340 \pm 60 \text{ nm}$  were observed and attributed to dislocation re-arrangement (Ref 30).

Nanoindentation was used to measure the hardness of the Ni powder and coating. The average nano-hardness of the cross section of Ni powder and Ni coating was  $2.1 \pm 0.2$  and  $4.8 \pm 0.7 \text{ GPa}$ , respectively. This is related to the extensive plastic deformation leading to an increase in dislocation density and grain refinement in cold-sprayed coatings (Ref 10). Non-uniform microstructure caused an inhomogeneous distribution of hardness. The particle interface regions displayed higher hardness compared to that of the central regions due to more grain refinement. The Ni coating displayed a micro-hardness of  $345 \pm 17 \text{ HV1 kg}$  ( $3.4 \pm 0.2 \text{ GPa}$ ), which was significantly lower when compared to nano-hardness value ( $4.8 \pm 0.7 \text{ GPa}$ ).

**Fig. 2** (a) Cumulative velocity distribution for Ni particle in gas stream, (b) cross-sectional morphology and (c) top-down morphology of Ni coating

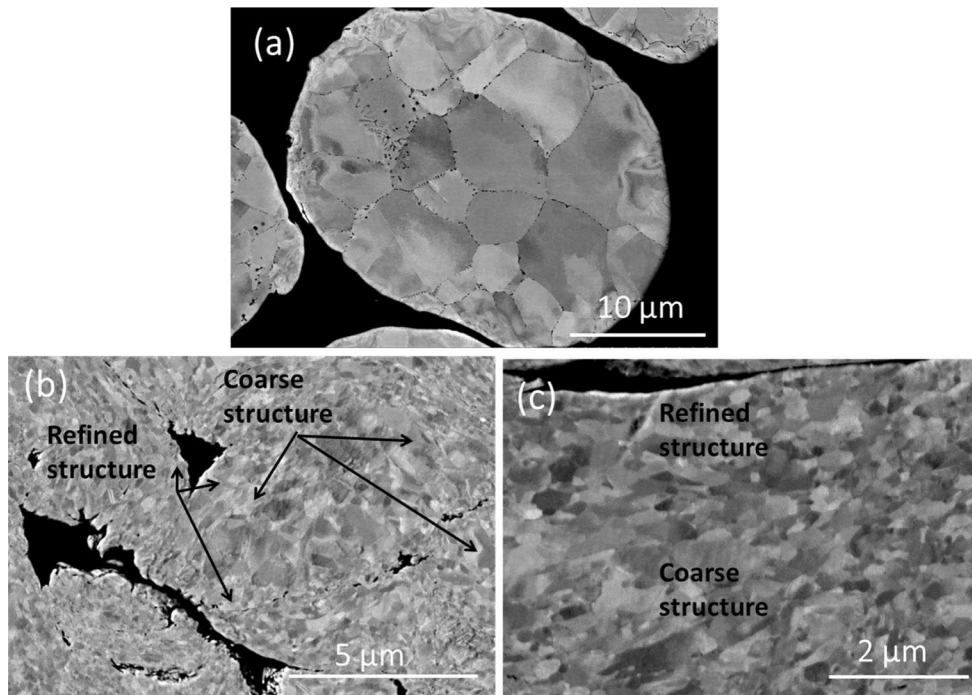
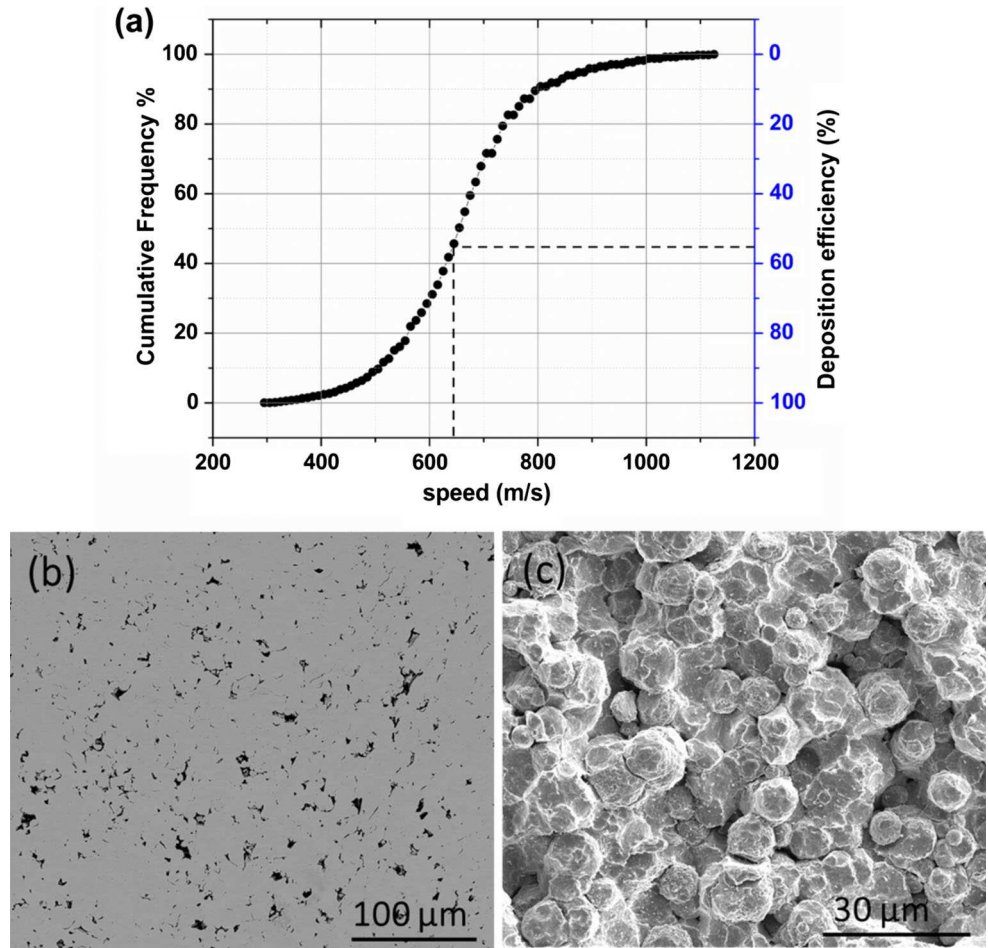


**Fig. 3** ECC imaging of cross section of (a) Ni powder, and (b) Ni coating, (c) high magnification view of (b)

### Ni-WC Coatings

The Ni-WC coatings were sprayed using three particle size distributions of WC with 36 vol.% WC in the feedstock. The WC fraction in the coatings, overall DE, partial DE of Ni and WC particles, and porosity of coatings are reported in Table 2. Comparing the WC fractions in the coatings, a higher retention of WC was achieved using the WC(30) powder. Similar results were reported in previous studies where finer size ceramic particles were more retained in coatings (Ref 18-20). However, with the finer WC(15), WC retention in coatings was not improved. The addition of WC into the initial mixture resulted in a lower DE of Ni, which can be due to WC fragments preventing close contact between previously deposited and impacting Ni. The overall DE and partial DEs of Ni and WC particles using similar WC contents in the feedstock were greater using finer WC particles. A reduction in the deposition buildup of the metallic phase when adding ceramic particles to the initial feedstock has been reported in previous studies (Ref 18, 20). The Ni-WC(30) coatings with higher WC contents of 50 and 80 vol.% in the feedstock powders showed an increase in the WC content in the coatings. However, as the ceramic particle content in the feedstock is increased, interactions between ceramic particles during deposition become more frequent, which led to a reduction in overall DE, as well as partial DE of Ni and WC.

Figure 4 shows micrographs of cross-sectioned Ni-WC composite coatings. For all three WC sizes tested, some WC particles cracked or fragmented upon impact. To examine this further, a fragmentation fraction was defined as  $\frac{\text{overall WC vol.\%} - \text{intact WC vol.\%}}{\text{overall WC vol.\%}}$ . More severe fragmentation and cracking ( $74\% \pm 8$ ) were observed in the larger size WC(40) compared to WC(30) and WC(15), which had fragmentation fractions of  $48\% \pm 12$  and  $25\% \pm 5$ , respectively. However, at higher WC(30) contents, fragmentation fractions were higher and almost all of the WC particles were cracked/fragmented. The top view images of Ni-10.5WC(30), shown in Fig. 4(f),

demonstrate that adding WC particles into the feedstock greatly altered the coating compared to Ni coatings (Fig. 2c). Interfaces between individual Ni particles were not easily visible due to improved adhesion and densification by the tamping effect of dense WC particles (Ref 11). Most of the WC particles rebounded after impacting the surface, leaving behind empty craters, which led to low retention of WC. There were also many fine pieces of fragmented WC particles that can be observed on the top surface (Fig. 4f).

### Ni-WC/Ni Coatings

For the Ni-WC/Ni coatings, Table 3 summarizes the WC fraction, overall DE, partial DE of Ni and WC, and porosity. Figure 5 shows micrographs of cross-sectioned Ni-WC/Ni composite coatings sprayed using various WC/Ni contents in the feedstock. Using WC/Ni composite powder, the retention of WC in the coating was significantly improved and the WC content was close to that of the initial feedstock composition. This is related to the porous and agglomerated structure of the powder, which allows particle densification and deformation during deposition (Ref 13-17). Voids present between aggregated WC particles in the WC/Ni powder, along with porosity inside the powders and Ni binder between WC agglomerates, provide ductility. Upon impact at high velocity, compaction and deformation of WC/Ni particles near the contact area occurred through slipping and rotation of WC particles along the Ni binder. This is referred to as the pseudo-deformation of the particles (Ref 13). As WC/Ni content in the initial feedstock increased, the overall DE decreased. With 95 vol.% WC/Ni added to the initial Ni powder (76 vol.% WC in total), a thin coating with lateral cracks along lamellar interfaces was obtained (Fig. 5d). When using WC/Ni powders as feedstock, with no Ni addition, the DE was very low and only a few of highly deformed and flattened particles with lateral cracks were deposited onto the substrate (Fig. 5e and f).

**Table 2** Characteristics of cold-sprayed Ni and Ni-WC coatings

Sample designation	DE, %			WC in feedstock powder, vol.%	WC in coatings, vol.%	Porosity, %
	Overall DE, %	Ni DE, %	WC DE, %			
Ni	55 ± 3	55 ± 3	...	...	...	3.8 ± 0.5
Ni-5.4WC(40)	12 ± 4	18 ± 6	2 ± 1	36	5.4 ± 0.7	0.9 ± 0.1
Ni-9.5WC(15)	20 ± 5	28 ± 7	5 ± 1	36	9.5 ± 0.5	1.7 ± 0.2
Ni-10.5WC(30)	22 ± 4	31 ± 6	6 ± 1	36	10.5 ± 0.9	1.1 ± 0.2
Ni-16WC(30)	15 ± 6	25	5	50	16 ± 2	0.5 ± 0.1
Ni-28WC(30)	5 ± 3	18.5	1.6	80	28 ± 4	0.3 ± 0.1

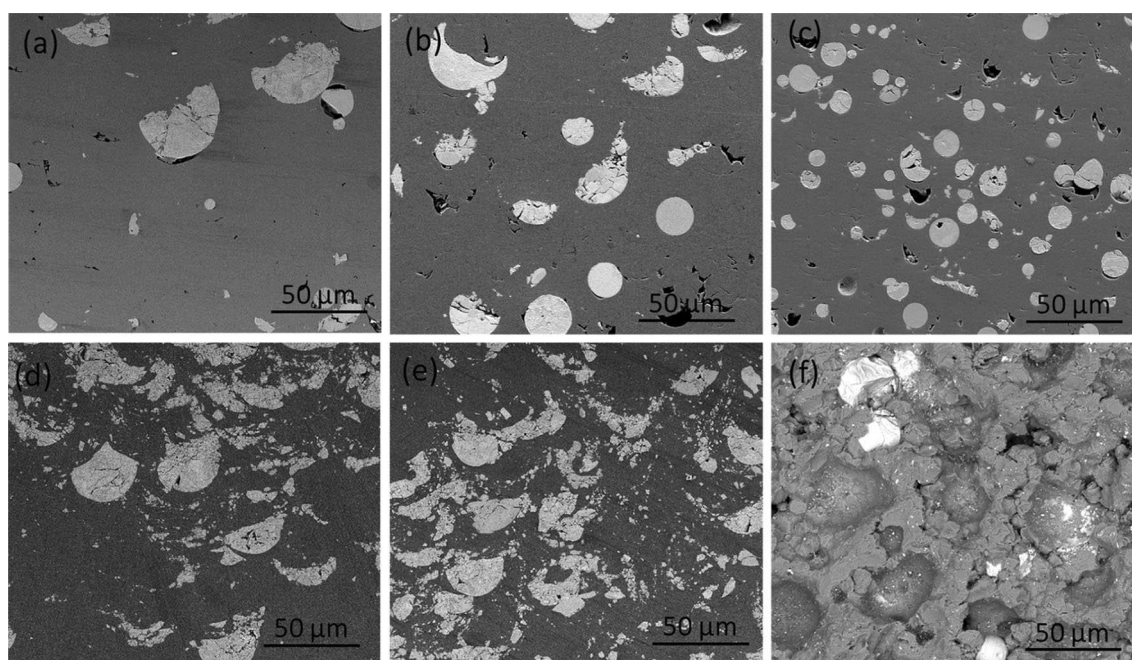


**Fig. 4** Cross-sectional morphology of (a) Ni-5.4WC(40), (b) Ni-10.5WC(30), (c) Ni-9.5WC(15), (d) Ni-16WC(30), (e) Ni-28WC(30) coatings, and (f) top-down morphology of Ni-10.5WC(30) coating

**Table 3** Characteristics of cold-sprayed Ni-WC/Ni coatings

Sample designation	DE, %			WC in feedstock powder, vol.%	WC in coatings, vol.%	Porosity, %
	Overall DE	Ni DE	WC DE			
Ni-13WC/Ni	75 ± 4	98 ± 5	59 ± 14	20	13 ± 3	0.9 ± 0.2
Ni-30WC/Ni	67 ± 5	73 ± 5	55 ± 10	36	30 ± 5	0.5 ± 0.2
Ni-43WC/Ni	44 ± 9	52 ± 11	36 ± 9	52	43 ± 7	0.4 ± 0.1
Ni-54WC/Ni	20 ± 8	38 ± 15	14 ± 6	76	54 ± 7	0.9 ± 0.2
WC/Ni	...	...	...	81	81	1.2 ± 0.5

The addition of WC/Ni to Ni not only resulted in a higher retention of WC in coatings, when compared to Ni-WC coatings (see section [Ni-WC Coatings](#)), but also improved partial DE of Ni at 36 and 52 vol.% WC in the initial feedstock. This contrasts with the reduction in the DE of Ni with the addition of the cast WC particles. Figure 6(a) and (c) shows the top surface morphology of Ni-30WC/Ni and Ni-54WC/Ni coatings, respectively. Previous studies reported partial compaction of porous WC/Co particles near the interface between the particle and the underlying coating (Ref 13). On the other hand, the compaction near the free surface of these particles is much more limited (Ref 13), which provides a deformable porous surface layer for the impacting Ni particles (see Fig. 6a and b). However, as the WC/Ni content in the feedstock is increased, the DE of Ni, as well as DE of WC/Ni particles, slightly decreased (see Fig. 6c).

The addition of WC/Ni to Ni in the feedstock powders resulted in decreased coating porosity. All the cold-sprayed Ni-WC/Ni coatings exhibited porosity less than 1%. The porosity in WC/Ni and Ni-54WC/Ni coatings with the initial 76 vol.% WC was due to cracking and debonding of splats.

### Hardness of Composite Coatings

Micro-hardness testing was performed on the polished top surfaces of cold-sprayed Ni and composite coatings. Micro-hardness results are plotted as a function of WC content in the coatings in Fig. 7. There are several factors that could contribute to the hardness of composite coatings by the addition of the WC particles including: densification caused by the tamping effect of impacting ceramics (Ref 11), load-bearing effects by ceramic particles (Ref 31), and

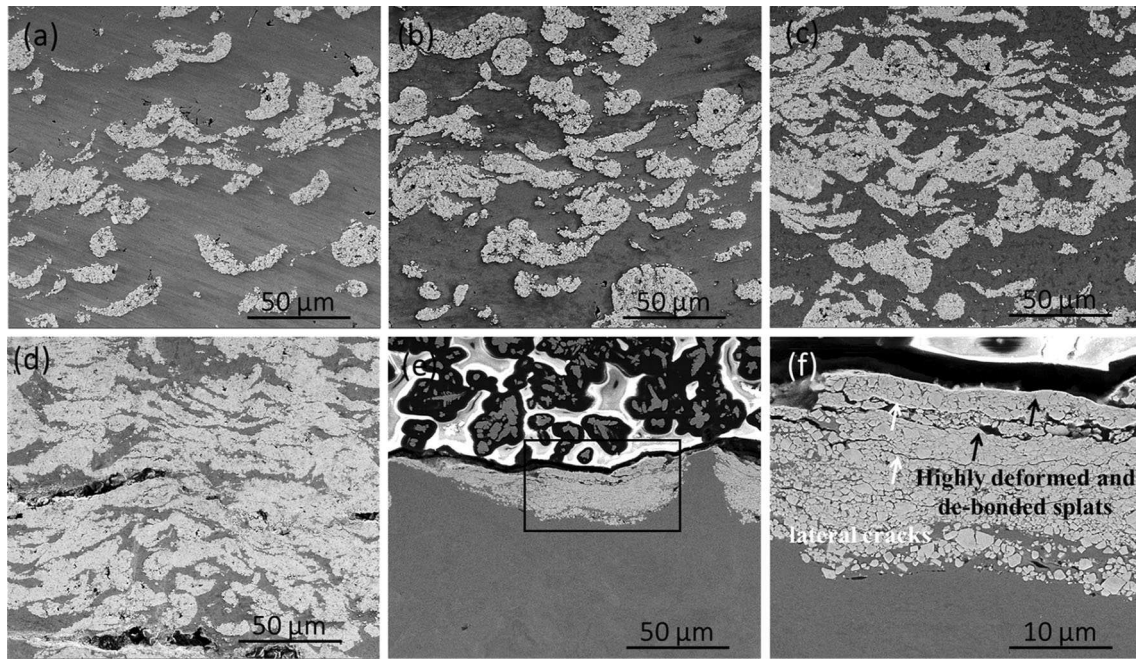


**Fig. 5** Cross-sectional morphology of (a) Ni-13WC/Ni, (b) Ni-30WC/Ni, (c) Ni-43WC/Ni, (d) Ni-54WC/Ni, (e) WC/Ni coatings, and (f) high magnification view of (e)

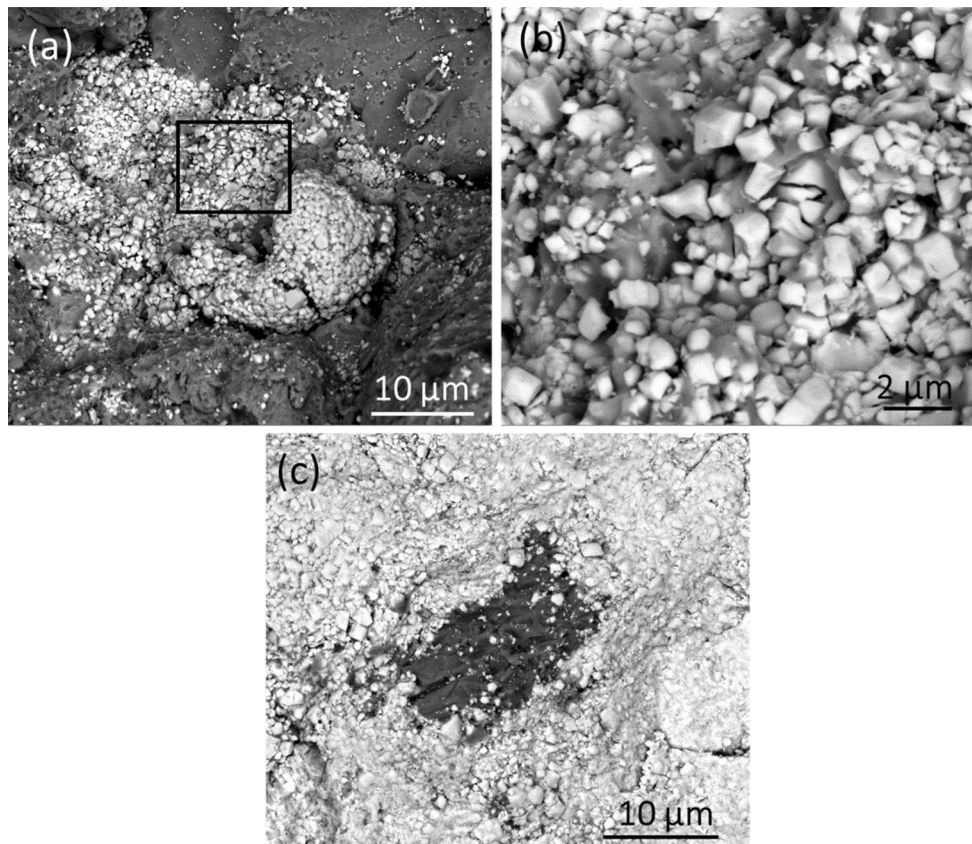


**Fig. 6** Top-down morphology (a) and (c) of the Ni-30WC/Ni and Ni-54WC/Ni coatings, respectively, (b) high magnification view of (a)

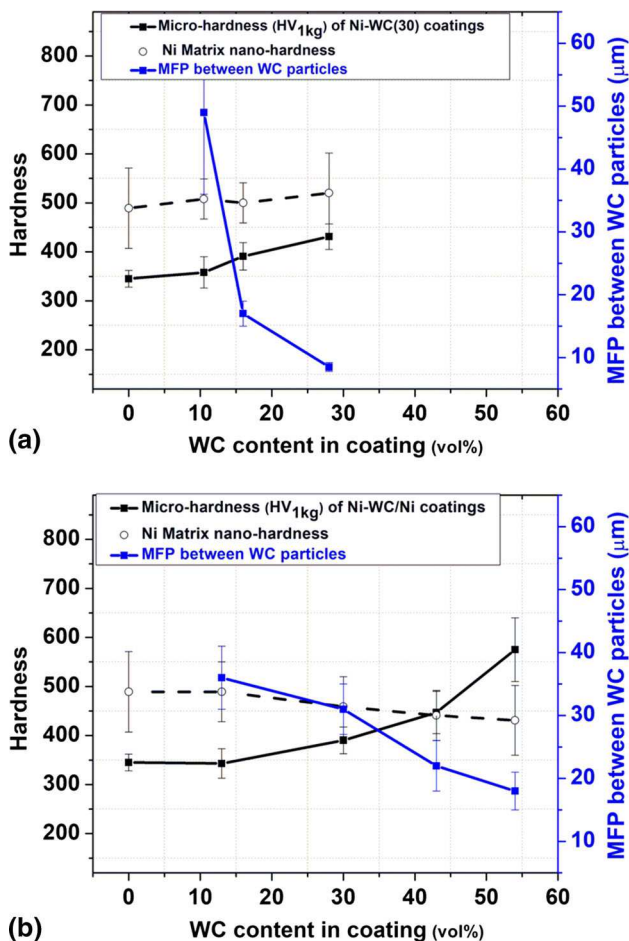


**Fig. 7** Vickers micro-hardness of coatings, nano-hardness of Ni matrices, and mean free path between WC particles vs. WC content for (a) Ni-WC(30), and (b) Ni-WC/Ni coatings

increased dislocation density and work hardening of the matrix caused by ceramic impacts (Ref 31). To further analyze the change in Ni matrix hardness caused by ceramic impacts, the nano-hardness of the Ni matrices was measured for composite coatings and compared to that of the Ni coating. Previous studies (Ref 26, 27) showed that the mean free path (MFP) between reinforcing particles directly influenced the mechanical properties of MMCs. In Fig. 7, the MFP between reinforcing particles and nano-hardness of the Ni matrices for composite coatings was plotted versus WC content in the coatings.

For the two types of WC particles tested in this study, the decrease in the coating porosity due to the tamping effect resulted in the increase in the coating micro-hardness. The addition of WC particles to the coatings plays two competitive roles on the strength of bonding between Ni splats as well as Ni/WC particles. While it strengthens the Ni matrix–matrix bonding due to the increased plastic deformation, it also leads to an increasing proportion of weaker matrix–ceramic particles. Another factor that could

contribute to the increase in micro-hardness of the composite coatings is the supporting role of WC particles to the load and reinforcing Ni matrix against plastic deformation. However, as mentioned above, weak interfacial bonding between Ni and WC particles limits the load transfer to the reinforcing particles. Moreover, cracking and fragmentation of WC particles upon impact led to loose WC fragments with reduced load-bearing capabilities. Work hardening of the matrix phase caused by the impact of the ceramic phase could also be a possible factor influencing the hardness of composite coatings. Nano-hardness measurements of Ni matrices in composite coatings showed that the addition of lower contents of cast WC to the coating did not change the nano-hardness of the Ni matrices significantly. The increased nano-hardness of the Ni matrix in Ni-28WC(30) coatings is due to ultra-fine ( $< 1 \mu\text{m}$ ) WC fragments. Compared to that of the Ni coating, slightly lower nano-hardness in the Ni matrix of Ni-43WC/Ni and Ni-54WC/Ni was recorded.

Higher WC contents were more effective in increasing micro-hardness of the composite coatings. This is attributed to the lower MFP between reinforcing particles in which the densification, as well as load-bearing effect of WC particles, was more effectively realized.

## Discussion

### DE, Microstructure, and Hardness of Ni Coating

Ni particles were accelerated to an average velocity of  $650 \pm 125 \text{ m/s}$ . Velocities of particles in the gas stream vary inversely with the square root of particle diameter, and thus, finer particles attain higher impact velocities (Ref 9). According to previous studies (Ref 29, 32), the critical velocities can be calculated by correlating the deposition efficiencies with particle impact velocities. A critical velocity for the successful deposition of Ni was calculated to be 550–650 m/s for a 25- $\mu\text{m}$  powder size (Ref 32, 33). The critical velocity for the Ni powder ( $d_{50} = 7 \mu\text{m}$ ) tested in the present study was found to be 650–670 m/s. This range of values is higher than other reported critical velocities for Ni powder due to the smaller Ni particles size used in this study. Previous studies showed that shear instabilities in smaller metallic particles can be hindered because of higher cooling rates during impact and intensified strain rate hardening (Ref 30). Another probable reason could be the higher amounts of surface contaminations in smaller size particles, such as oxide, which can have a negative effect on bonding (Ref 32).

A significant increase in hardness value of the Ni coating ( $4.8 \pm 0.7 \text{ GPa}$ ) compared to that of the Ni feedstock powder ( $2.1 \pm 0.2 \text{ GPa}$ ) was recorded, which is tied to the

increased dislocation density and grain refinement. The microstructure of Ni coating is non-uniform and near particle interfaces, cell structures with an average size of  $340 \pm 60$  nm can be observed (Fig. 3b and c) due to dislocation re-arrangement. High strain and high strain rate deformed microstructures are characterized by dislocation cells as most common type of low energy dislocation structure (LEDS) (Ref 34, 35). Mur et al, (Ref 34) estimated the dislocation cells diameter ( $d$ ) using the following equation,

$$(\tau - \tau_0) = KGb/d \quad (\text{Eq 1})$$

where  $\tau$  is shear stress,  $\tau_0$  is friction shear stress,  $G$  is shear modulus (76 GPa for Ni),  $b$  is Burgers vector (0.3 nm for Ni), and  $K$  is a factor with a value near 10. Using Taylor factor ( $M$ ) which is near 2.8, the term  $(\tau - \tau_0)$  can be calculated from  $(\sigma - \sigma_0)$ , (Ref 36)

$$(\sigma - \sigma_0) = M(\tau - \tau_0) \quad (\text{Eq 2})$$

where  $\sigma$  is applied stress, and  $\sigma_0$  is friction stress. According to Borchers et al., (Ref 30)  $\sigma$  in cold spray is estimated by,

$$\sigma = \frac{1}{2} \rho v^2 \quad (\text{Eq 3})$$

where  $\rho$  is density (8908 kg/m<sup>3</sup>) and  $v$  is particle velocity (650 m/s). Assuming  $\sigma_0$  is about 10-30% of the applied stress value for close-packed pure metals, (Ref 36) the dislocation cell diameter can be calculated to be within the range of 315-400 nm. This is consistent with the  $340 \pm 60$  nm observed from ECC images.

The micro-indentation measurements showed a lower hardness value of  $345 \pm 17$  HV<sub>1kg</sub> ( $3.8 \pm 0.2$  GPa) in comparison to the nano-hardness of the coating ( $4.8 \pm 0.7$  GPa). This is due to a larger scale indentation, where porosity and poor cohesive strength between cold-sprayed Ni particles led to a lower hardness. Goldbaum et al. (Ref 37) formulated a hardness loss parameter that helped explain the mechanical behavior at wide length scales and its relation to the various defects within the Ti coatings, such as porosity and poor particle adhesion.

### Effect of WC Powder Size on WC Retention in Coatings

WC does not plastically deform upon impact but becomes embedded in the substrate and is entrapped by matrix particles. Several factors, including substrate/matrix deformation properties, WC particle size and shape, affect its retention in coatings. During cold spraying, there is a stream of powder impacting the surface over a very short time. Entrapment by later arriving Ni particles, which deform and capture the rebounding WC in the coating, can

be an active mechanism (Ref 24). However, the interaction between particles in cold spray has not been widely studied yet. In most studies of cold spray, isolated impacts were considered (Ref 9, 32, 38). During impact of WC on Ni splats, impact loading applied to Ni causes it to deform. This can lead to shear localization at the interface (Ref 31, 39) and the formation of craters and jetting around the periphery of the craters. A large number of empty craters were observed on the top surface of Ni-WC coatings (Fig. 4e and f), which implies that the conditions required for WC particles to embed into the Ni were not entirely met for the powders and spray conditions used. Getu et al. (Ref 40) studied the embedding behavior of hard spherical and angular erodent particles into ductile polymer substrates during solid particle erosion (SPE) by modeling and experimental work. Embedding of spherical particles was predicted to be unlikely under normal impacts due to rebound forces being higher than the frictional forces that retain the particles (Ref 40). Their study considered much lower particles velocity ranges (1-150 m/s) (Ref 40) compared to those attained by cold-sprayed particles (e.g., 484-627 m/s in the present study). Nevertheless, the results are consistent with the low retention of spherical WC seen here.

Coarse WC particles impact the surface with higher impact energies and are expected to cause more plastic deformation of the substrate (Ref 29). A lower fraction of recovered WC particles as well as an increase in WC fragmentation using WC(40) particles was observed (see Fig. 4). Fragmentation dissipates a part of the kinetic energy of impacting particles that would otherwise be used for substrate plastic deformation and embedding (Ref 41). Ceramic particles undergo fragmentation upon impact above a certain threshold velocity, which depends on ceramic particle properties and decreases with increasing particle radius (Ref 42). This is due to the higher density of defects present in the coarser particles, which implies that fracture might be avoided by limiting the ceramic size. A higher fraction of recovered WC particles, as well as a reduction in WC fragmentation (see Fig. 4) using WC(30) and WC(15) particles, are consistent with the above explanation. However, using much smaller WC particles (15  $\mu\text{m}$ ) did not further improve WC retention. This can be due to the much lower kinetic energy attained by these particles (Ref 41), although fragmentation is significantly avoided. Moreover, higher porosity and relatively lower micro-hardness were recorded in the Ni-WC(15) coating, where the lower kinetic energy of particles was less effective in coating densification.

The ceramic particles can fragment upon impact for various reasons, including ceramic-ceramic interactions, the energy of impact of the ceramic particle alone, or the energy of later arriving metal/ceramic particles striking a

retained ceramic particle. Higher WC contents in the feedstock powders led to higher collisions of WC particles. This caused fragmentation of almost all of the WC particles in Ni-16 and 28WC(30) coatings and, in turn, led to reduced DE of Ni. Low Ni content in the feedstock, as well as low deposition rates of Ni in the two mentioned coatings, resulted in reduced DE of WC, although the WC content was higher compared to that of the Ni-10.5WC(30).

### Effect of WC Morphology on DE and WC Retention in Coatings

The porous and agglomerated structure of WC/Ni powders provided ductility during particle deformation (Ref 13–17). Moreover, the WC particles in the powder are bonded loosely by a metallic binder (Ref 13). The WC/Ni particle deforms easily upon impact through pseudo-deformation (Ref 13), which is associated with slipping of WC fragments along the metallic binder and densification. Yet, when spraying alone, the WC/Ni particles did not deposit well and coatings were thin with low DE. The addition of Ni to WC/Ni feedstock was found to improve coating deposition. For all the various initial WC/Ni contents in the Ni-WC/Ni tested in this study, 65–83% of WC particles were recovered in the coating compared to 24–36% achieved using cast WC(30) particles.

The deposition mechanism of WC-based particles during cold spray has not been investigated in detail. However, the mechanical interlocking of WC fragments in the underlying coating and/or adhesion between metallic phases in incoming WC/Co particles and the deposited layer were reported as active mechanisms (Ref 43). The two mechanisms have stringent conditions that are limited by the amount of Co binder available and/or deformability of the binder phase (Ref 44). Previous studies deposited WC-Co cermets using porous feedstock powder with sufficient binder/matrix content (Ref 13–16), powder preheating prior to spraying (Ref 17), and using a fixed spray gun (Ref 44). The deposition of a WC/Ni coating was not realized in the present study under tested conditions. Highly deformed and flattened particles were observed in the cross section of a WC/Ni coating; at some regions of which, the splats debonded from the surface (see Fig. 5e and f). The formation of a strong bond of impacting WC/Ni particles with the underlying coating is required for the successive buildup of a WC/Ni coating to a designed thickness. The creation of such cohesion is associated with attaining a certain degree of deformation of both the impacting particles and the underlying coating (Ref 13). Without Ni addition, the hard WC/Ni underlying coating prevents significant accommodation of shear deformation and causes impacting particles to be heavily deformed and flattened. Eventually, after a

part of the kinetic energy of the impacting WC/Ni particle was consumed by plastic deformation in both parts and any adhesive interaction, the rest is stored as elastic energy and causes the particle to bounce off the surface.

The addition of Ni into the initial feedstock was found to accommodate plastic deformation partly and prevent WC/Ni particles from rebounding. As reported by previous studies, the degree of deformation changes from the contact surface of impacting particle to its top surface. Significant deformation is limited to the regions close to contact surfaces (Ref 45). This leads to partial compaction of porous particles near the impact area (Ref 13). Upon impact of particles on such a WC/Ni layer during coating buildup, deformation of the top surface of the underlying coating and the bottom portion of impacting particle occurs. This led to an improvement in overall DE as well as retention of WC in coatings when compared to those using cast WC particles. Figure 8 shows a schematic illustration of different mechanisms by which WC/Ni and WC particles were retained in coatings.

Partial compaction of WC/Ni particles at lower ceramic contents, as mentioned above, helped in the deposition of Ni particles when compared to a Ni coating alone. However, heavily deformed and flattened WC/Ni particles, using high WC content in the feedstock, were not effective in improving the DE of Ni.

The deposition of Ni-WC/Co composite coatings has been reported in previous studies by other authors, where low-pressure cold spray systems were used (Ref 26, 27). The retention of WC in Ni-WC/Ni coatings in the present study is compared to those in Ni-WC/Co coatings reported in previous studies in Fig. 9. A higher retention of WC was obtained in the present study using a high-pressure cold spray system. This can be related to higher velocities attained by the WC/Ni particles, which causes a higher degree of plastic deformation in both Ni and WC/Ni particles and deposition of coatings with nearly theoretical densities. In comparison, higher porosity levels were reported for similar coatings using the low-pressure cold spray (up to 5%), which is associated with a lower impact velocity of particles (Ref 26, 27). The higher recorded porosity for WC/Ni and Ni-54WC/Ni with 76 vol.% WC in the feedstock is believed to be due to the excessive kinetic energy and debonding of highly deformed splats, not lack of deformation.

### Effect of the WC Particles on Hardness of the Composite Coatings

Micro-hardness measurements of composite coatings showed that as the WC content in the coating increased, the micro-hardness increased, which is related to the reduced mean free path between WC/Ni particles in higher content

**Fig. 8** A schematic graph showing how (a) cast WC, (b) WC/Ni particles were retained in coatings. Gray and white represent WC and Ni particles, respectively

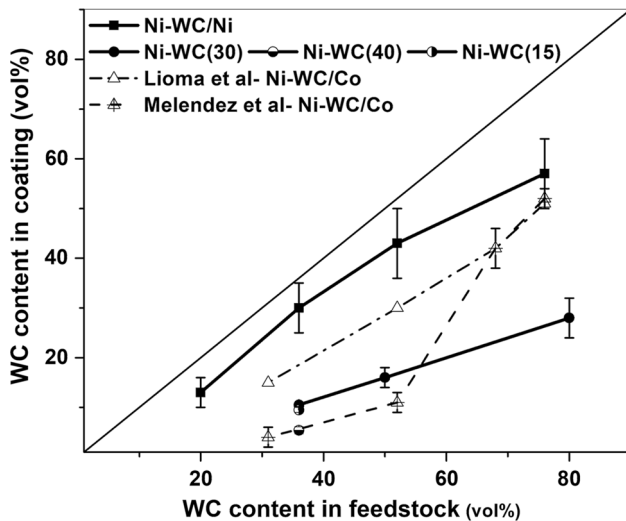
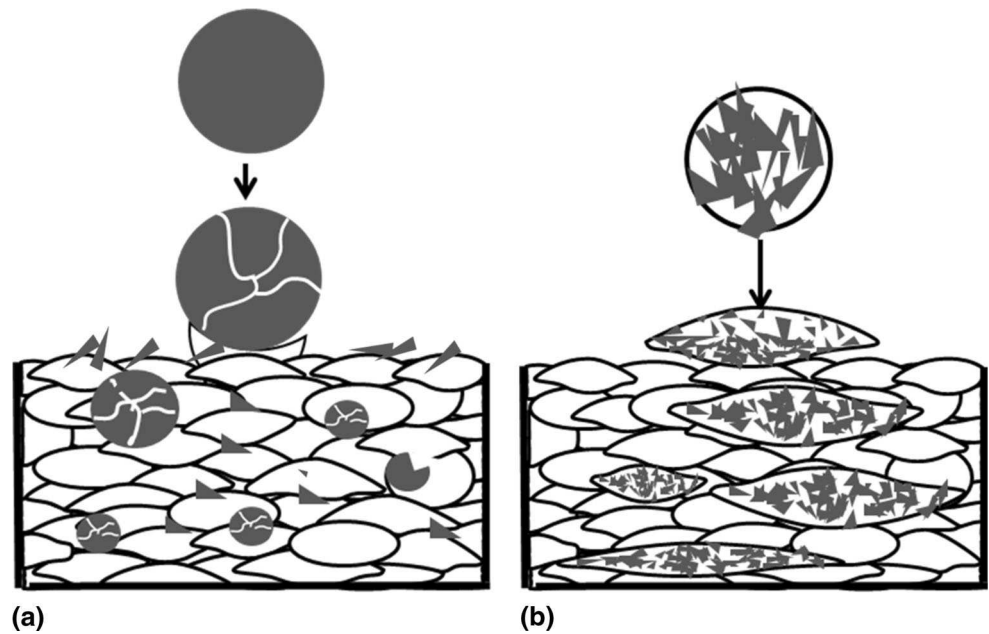


**Fig. 9** WC content in the coating vs. WC content in the feedstock powder (solid line-bold symbols). Dashed and dashed-dotted lines represent previous results (Ref 26, 27)

WC coatings and the densification of coatings (Ref 26, 27). Comparing the micro-hardness values of the two composite coatings with similar WC content but different type,  $431 \pm 26 \text{ HV}_{1\text{kg}}$  for 28 WC vol.% Ni-28WC(30) vs.  $390 \pm 27 \text{ HV}_{1\text{kg}}$  for 30 WC vol.% Ni-30WC/Ni, cast WC particles were more effective in strengthening the coatings. This is due to a significantly lower MFP between WC fragments ( $8.5 \pm 0.7 \mu\text{m}$ ) in Ni-28WC(30) compared to that of the Ni-30WC/Ni coatings ( $31 \pm 4 \mu\text{m}$ ). Another possible reason could be the harder cast WC powders ( $2461 \pm 331 \text{ HV}_{25\text{g}}$ ) when compared to WC/Ni powders ( $601 \pm 168 \text{ HV}_{25\text{g}}$ ), although the WC/Ni particles

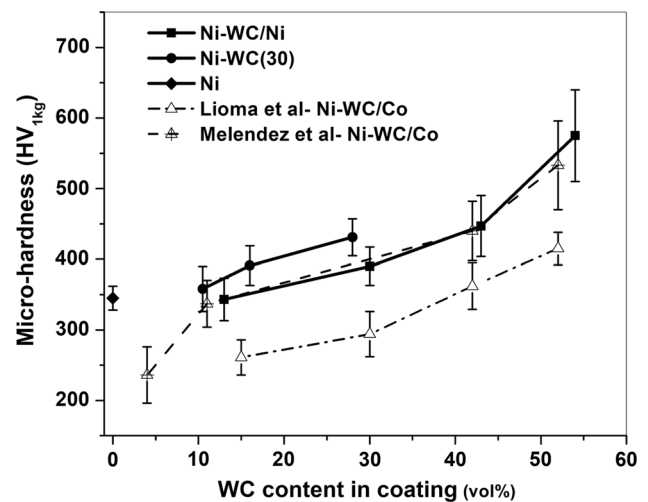


**Fig. 10** Vickers micro-hardness vs. WC content in the coating (solid line-bold symbols). Dashed and dashed-dotted lines represent previous results (Ref 26, 27)

hardness was significantly increased due to densification during impact.

The hardness of the composite coatings in the present study was compared to those of Ni-WC/Co obtained using the low-pressure cold spray in previous studies (Ref 26, 27) in Fig. 10. The Ni-WC/Ni coatings featured similar hardness values to those obtained by Melendez et al. (Ref 27). They reported similar porosities but lower MFP compared to those obtained in this study, for the coatings with similar WC contents. The hardness values for the coatings obtained by Lioma et al. (Ref 26) were lower than those obtained by Melendez et al. (Ref 27) and in this work. This effect is related to the higher porosity in the coatings

deposited in the Lioma et al. study (Ref 26) due to lower velocity attained by particles. A difference in the hardness and composition of the WC-based composite powders used in these two studies may also play a role. However, no hardness value for WC/Co powder was reported in the two previous studies.

Significantly harder WC-Ni and WC-Co composite coatings have been deposited using HVOF technology using similar feedstock powders (Ref 16, 46, 47). The HVOF coatings were thicker and harder than cold-sprayed coatings, using similar feedstock composition, due to the decomposition of the WC-based powder and formation of hard  $W_2C$  and  $Ni_6/Co_6W_6C$  or  $Ni_3/Co_3W_3C$  ( $\eta$ ) phases (Ref 16, 46). HVOF coatings are characterized as more brittle when compared to cold-sprayed coatings, due to the depletion of the ductile Co matrix and the presence of fragile and hard phases such as  $W_2C$ , W and/or  $\eta$  phases (Ref 16, 46). However, previous studies demonstrated that hardness is not the sole indicator of the ability of coatings to withstand wear (Ref 5, 6). Melendez et al. (Ref 48) studied dry abrasion wear performance of low-pressure cold-sprayed Ni and Ni-WC/Co composite coatings containing 7–66 wt.% WC. They reported that that cold-sprayed Ni-WC/Co coatings containing 66 wt.% WC can compete with an HVOF WC-12Co coating in terms of abrasive wear resistance, although the latter had a higher hardness ( $\sim 1100$  versus  $533 \pm 63$  HV) (Ref 48).

## Conclusion

Cold spray was used to fabricate Ni and Ni matrix composites reinforced with WC particles. Two types of WC powders were tested: cast spherical WC as well as an agglomerated and sintered WC/Ni composite. The effect of WC powder size distributions on WC retention in the coatings was studied. The concentration of WC in sprayed coatings was lower than that of the feedstock for all mixtures. The size of the WC particles was found to affect its retention in the coating. Using small WC particles, Ni-WC coatings with a higher WC content were obtained. Adding WC to the feedstock powder decreased the DE of Ni. A lower DE for both Ni and WC was reported using a higher WC(30) content in the feedstock powder. The Ni-WC coatings with higher WC retained in the coatings displayed higher hardness when compared to Ni and Ni-10.5WC(30) coatings due to a lower porosity and MFP. A significant improvement in WC retention in coatings was obtained using WC/Ni agglomerated and sintered powder mixed with Ni. The WC content in Ni-WC/Ni coatings was close to that of the initial feedstock. It was found that Ni-WC/Ni coatings can be tailored to contain 13–54 vol.% WC and display a varied hardness ranging between 343 and 575

HV. The addition of WC/Ni to the feedstock did not deteriorate deposition buildup of Ni particles. Rather, an improving effect of the DE of Ni at lower WC/Ni content in the feedstock was observed.

**Acknowledgments** The authors gratefully acknowledge the financial support from the Canadian Foundation for Innovation (CFI) project No. 8246 for the cold spray equipment, the CFI Leader's Opportunity Fund project No. 13029 for the tribometer and nanoindentation equipment, and the Natural Sciences and Engineering Research Council (NSERC) Strategic Grants Program for the operational funding of this project. Thanks, are also due to Tekna Inc for providing the Ni and spherical WC powders.

## References

1. M.R. Fernández, A. García, J.M. Cuetos, R. González, A. Noriega, and M. Cadenas, Effect of Actual WC Content on the Reciprocating Wear of a Laser Cladding NiCrBSi Alloy Reinforced with WC, *Wear*, 2015, **324–325**, p 80–89
2. K. Van Acker, D. Vanhoyweghen, R. Persoons, and J. Vangrunderbeek, Influence of Tungsten Carbide Particle Size and Distribution on the Wear Resistance of Laser Clad WC/Ni Coatings, *Wear*, 2005, **258**, p 194–202
3. J.M. Miguel, J.M. Guilemany, and S. Vizcaino, Tribological Study of NiCrBSi Coating Obtained by Different Processes, *Tribol. Int.*, 2003, **36**, p 181–187
4. P.L. Hurricks, Some Aspects of the Metallurgy and Wear Resistance of Surface Coatings, *Wear*, 1972, **22**, p 291–320
5. H. Wang, W. Xia, and Y. Jin, A Study on Abrasive Resistance of Ni-Based Coatings with a WC Hard Phase, *Wear*, 1996, **195**, p 47–52
6. P. Kulu and T. Pihl, Selection Criteria for Wear Resistant Powder Coatings Under Extreme Erosive Wear Conditions, *J. Therm. Spray Technol.*, 2002, **11**(4), p 517–522
7. M.R. Ramesh, S. Prakash, S.K. Nath, P.K. Sapra, and B. Venkataraman, Solid Particle Erosion of HVOF Sprayed WC-Co/NiCrFeSiB Coatings, *Wear*, 2010, **269**, p 197–205
8. D.A. Stewart, P.H. Shipway, and D.G. McCartney, Abrasive Wear Behaviour of Conventional and Nanocomposite HVOF-Sprayed WC-Co Coatings, *Wear*, 1999, **225–229**, p 789–798
9. A. Papyrin, V. Kosarev, S. Klinkov, A. Alkhimov, and V. Fomin, *Cold spray technology*, Elsevier, Amsterdam, 2006
10. Y. Zou, D. Goldbaum, J.A. Szpunar, and S. Yue, Microstructure and Nanohardness of Cold-Sprayed Coatings: Electron Backscattered Diffraction and Nanoindentation Studies, *Scripta Mater.*, 2010, **62**, p 395–398
11. F. Sevillano, P. Poza, C.J. Múñez, S. Vezzú, S. Rech, and A. Trentin, Cold-Sprayed Ni- $Al_2O_3$  Coatings for Applications in Power Generation Industry, *J. Therm. Spray Technol.*, 2013, **22–5**, p 772–782
12. J. Wang and J. Villafuerte, *Processing and properties of advanced ceramics and composite*, Wiley, London, 2009
13. C.J. Li, G.J. Yang, P.H. Gao, J. Ma, Y.Y. Wang, and C.-X. Li, Characterization of Nanostructured WC-co Deposited by Cold Spraying, *J. Therm. Spray Technol.*, 2007, **16**, p 1011–1020
14. R. Lima, J. Karthikeyan, C.M. Kay, J. Lindemann, and C.C. Berndt, Microstructural Characteristics of Cold-Sprayed Nanostructured WC-Co Coatings, *Thin Solid Films*, 2002, **416**, p 129–135
15. P.H. Gao, Y.G. Li, C.J. Li, G.J. Yang, and C.X. Li, Influence of Powder Porous Structure on the Deposition Behavior of Cold-

- Sprayed WC-12Co Coatings, *J. Therm. Spray Technol.*, 2008, **17**, p 742-749
16. M. Couto, S. Dosta, M. Torrell, J. Fernández, and J.M. Guilemany, Cold Spray Deposition of WC-17 and 12Co Cermets onto Aluminum, *Surf. Coat. Technol.*, 2013, **235**, p 54-61
  17. H.J. Kim, C.H. Lee, and S.Y. Hwang, Fabrication of WC-Co Coatings by Cold Spray Deposition, *Surf. Coat. Technol.*, 2005, **191**, p 335-340
  18. A. Sova, V.F. Kosarev, A. Papyrin, and I. Smurov, Effect of Ceramic Particle Velocity on Cold Spray Deposition of Metal-Ceramic Coatings, *J. Therm. Spray Technol.*, 2011, **20**(1–2), p 285-291
  19. A. Sova, A. Papyrin, and I. Smurov, Influence of Ceramic Powder Size on Process of Cermet Coating Formation by Cold Spray, *J. Therm. Spray Technol.*, 2009, **18**(5–6), p 633-641
  20. H. Koivuluoto and P. Vuoristo, Effect of Ceramic Particles on Properties of Cold-Sprayed Ni-20Cr + Al<sub>2</sub>O<sub>3</sub> Coatings, *J. Therm. Spray Technol.*, 2009, **18**(4), p 555-562
  21. M. Yu, X.K. Suo, W.Y. Li, Y.Y. Wang, and H.L. Liao, Microstructure, Mechanical Property and Wear Performance of Cold Sprayed Al5056/SiCp Composite Coatings: Effect of Reinforcement Content, *Appl. Surf. Sci.*, 2014, **289**, p 188-196
  22. O. Meydanoglu, B. Jodoin, and E.S. Kayali, Microstructure, Mechanical Properties and Corrosion Performance of 7075 Al Matrix Ceramic Particle Reinforced Composite Coatings Produced by the Cold Gas Dynamic Spraying Process, *Surf. Coat. Technol.*, 2013, **235**, p 108-116
  23. M. Yu, W.Y. Li, X.K. Suo, and H.L. Liao, Effects of Gas Temperature and Ceramic Particle Content on Microstructure and Microhardness of Cold Sprayed SiCp/Al 5056 Composite Coatings, *Surf. Coat. Technol.*, 2013, **220**, p 102-106
  24. P.C. King, S.H. Zahiri, and M.Z. Jahedi, Rare Earth/Metal Composite Formation by Cold Spray, *J. Therm. Spray Technol.*, 2007, **17**–2, p 221-227
  25. J.M. Shockley, S. Descartes, P. Vo, E. Irissou, and R.R. Chromik, The Influence of Al<sub>2</sub>O<sub>3</sub> Particle Morphology on the Cold Spray Coating Formation and Dry Sliding Wear Behavior, *Surf. Coat. Technol.*, 2015, **270**, p 324-333
  26. D. Lioma, N. Sacks, and I. Bote, Cold Gas Dynamic Spraying of WC-Ni Cemented Carbide Coatings, *Int. J. Refract. Metals Hard. Mater.*, 2015, **49**, p 365-373
  27. N.M. Melendez and A.G. McDonald, Development of WC-Based Metal Matrix Composite Coatings Using Low-Pressure Cold Gas Dynamic Spraying, *Surf. Coat. Technol.*, 2013, **214**, p 101-109
  28. W.C. Oliver and G.M. Pharr, An Improved Technique for Determining Hardness and Elastic Modulus Using Load and Displacement Sensing Indentation Experiments, *J. Mater. Res.*, 1992, **7**–6, p 1564-1583
  29. E. Irissou, J.-G. Legoux, B. Arsenaault, and C. Moreau, Investigation of Al-Al<sub>2</sub>O<sub>3</sub> Cold Spray Coating Formation and Properties, *J. Therm. Spray Technol.*, 2007, **16**, p 661-668
  30. F. Borchert, T. Gärtner, T. Stoltenhoff, H. Assadi, and H. Kreye, Microstructural and Macroscopic Properties of Cold Sprayed Copper Coatings, *J. Appl. Phys.*, 2003, **93**, p 10064-10070
  31. X.K. Suo, Q.L. Suo, W.Y. Li, M.P. Planche, and H.L. Liao, Effects of SiC Volume Fraction and Particle Size on the Deposition Behavior and Mechanical Properties of Cold-Sprayed AZ91D/SiCp Composite Coatings, *J. Therm. Spray Technol.*, 2014, **23**(1–2), p 91-97
  32. T. Schmidt, F. Gärtner, H. Assadi, and H. Kreye, Development of a Generalized Parameter Window for Cold Spray Deposition, *Acta Mater.*, 2006, **54**, p 729-742
  33. T. Schmidt, H. Assadi, F. Gärtner, H. Richter, T. Stoltenhoff, H. Kreye, and T. Klassen, From Particle Acceleration to Impact and Bonding in Cold Spraying, *J. Therm. Spray Technol.*, 2009, **18**(5–6), p 794-808
  34. L.E. Murr, C.-S. Niou, S. Pappu, J.M. Rivas, and S.A. Quinones, LEDS in Ultra-High Strain-Rate Deformation, *Phys. Stat. Sol. A*, 1995, **149**, p 253-274
  35. B. Bay, N. Hansen, D.A. Hughes, and D. Kuhlmann-Wilsdorf, Overview no. 96 Evolution of f.c.c. Deformation Structures in Polyslip, *Acta Mater.*, 1992, **40**, p 205-219
  36. H. Burt, J.P. Dennison, and B. Wilshire, Friction Stress Measurements During Creep of Nimonic 105, *Mater. Sci.*, 1979, **13**(5), p 295-300
  37. D. Goldbaum, J. Ajaja, R.R. Chromik, W. Wong, S. Yueb, E. Irissou, and J.-G. Legoux, *Mater. Sci. Eng. A*, 2011, **530**(1), p 253-265
  38. H. Assadi, F. Gärtner, T. Stoltenhoff, and H. Kreye, Bonding Mechanism in Cold Gas Spraying, *Acta Mater.*, 2003, **51**(15), p 4379-4394
  39. M. Grujicic, C. Zhao, W. DeRosset, and D. Helfrich, Adiabatic Shear Instability Based Mechanism for Particles/Substrate Bonding in the Cold-Gas Dynamic-Spray Process, *Mater. Des.*, 2004, **25**, p 681-688
  40. H. Getu, J.K. Spelt, and M. Papini, Conditions Leading to the Embedding of Angular and Spherical Particles During the Solid Particle Erosion of Polymers, *Wear*, 2012, **292**–293, p 159-168
  41. B. Daneshian and H. Assadi, Impact Behavior of Intrinsically Brittle Nanoparticles: A Molecular Dynamics Perspective, *J. Therm. Spray Technol.*, 2013, **23**(3), p 541-550
  42. E.W. Andrews and K.-S. Kim, Threshold Conditions for Dynamic Fragmentation of Ceramic Particles, *Mech. Mater.*, 1998, **29**, p 161-180
  43. A.S.M. Ang, C.C. Berndt, and P. Cheang, Deposition Effects of WC Particle Size on Cold Sprayed WC-Co Coatings, *Surf. Coat. Technol.*, 2011, **205**, p 3260-3267
  44. P.H. Gao, C.J. Li, G.J. Yang, Y.G. Li, and C.X. Li, Influence of Substrate Hardness Transition on Built-Up of Nanostructured WC-12Co by Cold Spraying, *Appl. Surf. Sci.*, 2010, **256**, p 2263-2268
  45. Y. Zou, W. Qin, E. Irissou, J. Legoux, S. Yue, and J.A. Szpunar, Dynamic Recrystallization in the Particle/Particle Interfacial Region of Cold-Sprayed Nickel Coating: Electron Backscatter Diffraction Characterization, *Scripta Mater.*, 2009, **61**, p 899-902
  46. M. Couto, S. Dosta, and J.M. Guilemany, Comparison of the Mechanical and Electrochemical Properties of WC-17 and 12Co Coatings onto Al7075-T6 Obtained by High Velocity Oxy-Fuel and Cold Gas Spraying, *Surf. Coat. Technol.*, 2015, **268**, p 180-189
  47. L.-M. Berger et al., Microstructure and Properties of HVOF-Sprayed Chromium Alloyed WC-Co and WC-Ni Coatings, *Surf. Coat. Technol.*, 2008, **202**, p 4417-4421
  48. N.M. Melendez, V.V. Narulkar, G.A. Fisher, and A.G. McDonald, Effect of Reinforcing Particles on the Wear Rate of Low-Pressure Cold-Sprayed WC-Based MMC Coatings, *Wear*, 2013, **306**, p 185-195